Magnetization process of spin ice in a [111] magnetic field

S. V. Isakov,[1] K. S. Raman,[2] R. Moessner[3] and S. L. Sondhi[2]

[1]*Department of Physics, AlbaNova, Stockholm University, SE-10691 Stockholm, Sweden*
[2]*Department of Physics, Princeton University, Princeton, NJ 08544, USA and*
[3]*Laboratoire de Physique Théorique de l'Ecole Normale Supérieure, CNRS-UMR8549, Paris, France*

(Dated: February 2, 2008)

Spin ice in a magnetic field in the [111] direction displays two magnetization plateaux, one at saturation and an intermediate one with finite entropy. We study the crossovers between the different regimes from a point of view of (entropically) interacting defects. We develop an analytical theory for the nearest-neighbor spin ice model, which covers most of the magnetization curve. We find that the entropy is non-monotonic, exhibiting a giant spike between the two plateaux. This regime is described by a monomer-dimer model with tunable fugacities. At low fields, we develop an RG treatment for the extended string defects, and we compare our results to extensive Monte Carlo simulations. We address the implications of our results for cooling by adiabatic (de)magnetization.

I. INTRODUCTION

Recent experiments on the spin ice compounds[1,2] $Ho_2Ti_2O_7$ and $Dy_2Ti_2O_7$ have uncovered an intriguing set of phenomena when unicrystalline samples are placed in an external magnetic field in the [111] direction.[3,4,5,6] For a review on spin ice, see Ref. 7.

The discovery of a plateau in the magnetization below saturation, first predicted theoretically[8] and explored in Monte Carlo simulations,[8,9] has been particularly remarkable as it was found to retain a fraction of the zero-field spin ice entropy.[4,10,11] In this regime, the system is well described by a two-dimensional Ising model on a kagome lattice in a longitudinal field, which is in turn equivalent to a hexagonal lattice dimer model.[10,11,12].

Recently, two of the present authors have studied the thermodynamics and correlations of the [111] plateau.[11] This work has led to the identification of mechanisms which terminate the plateau. At the high-field end, the termination occurs via the proliferation of monomer defects in the underlying dimer model. At low fields, a more exotic extended string defect restores three dimensionality. The asymptotic density of both kinds of defects was estimated in Ref. 11.

In this paper, we consider in detail the full magnetization curve from zero-field to saturation. A brief synopsis of the exotic thermodynamic properties of spin ice is in a [111] field is sketched in Fig. 1. The aim of this paper is to identify the different regimes of the magnetization curves, to provide analytical theories for them, and to test them against Monte Carlo simulations, and finally against experiment.

Near zero field, we use the accurate self-consistent Hartree approximation[13] to provide an analytical approximation for the linear response regime. At the low field end of the plateau, we develop mean field and renormalization group treatments for the extended string defects, which we use to analyze the in-plane and out-of-plane correlations. We compare these with Monte Carlo simulations using an efficient cluster algorithm, which allows us to obtain accurate data from the linear response regime to the beginning of the [111] plateau. We find

that the mean field treatment is accurate at the lowest fields, where the string density would be relatively high. The renormalization group treatment compares well with simulation in the dilute string limit. At even higher fields, the plateau is approached and the suppression of the entropic activation of strings becomes apparent as a finite-size effect.

At the high-field termination of the plateau, we observe a giant peak in the entropy, which even exceeds the zero field Pauling value, despite the fact that a quarter of all spins are pinned. We model this phenomenon by a monomer-dimer model on the honeycomb lattice with varying fugacities. (At the point where the all fugacities equal 1, this model turns out to be one of 'hard bow-ties' on the kagome lattice.) We analyze this model within a Bethe approximation and also by using results from a high-order series expansion.[14]

We show that the entropy peak is due to the crossing of an extensive number of energy levels which have macroscopic entropies. Comparing this theory with Monte Carlo simulations of the appropriate monomer-dimer model, we find that the simple Bethe approximation is accurate for moderate to large monomer densities.

We point out that this theory predicts to a crossing point in the plots of magnetisation versus field at different temperatures. In addition, there is a further crossing point at lower fields, where the corrections to the magnetisation due to monomer and string defects almost cancel one another.

We then address the connection of these results to experiment, in particular pointing out the presence of (at least a vestige) of the entropy peak in existing experimental data.

We then discuss the implications of the entropy peak for magnetocaloric manipulations. In particular, we argue that it arises in a more general set of models. It can, in principle, be used to effect cooling in a field, both by adiabatic demagnetization, and by adiabatic magnetization. Finally, we close with some concluding remarks.
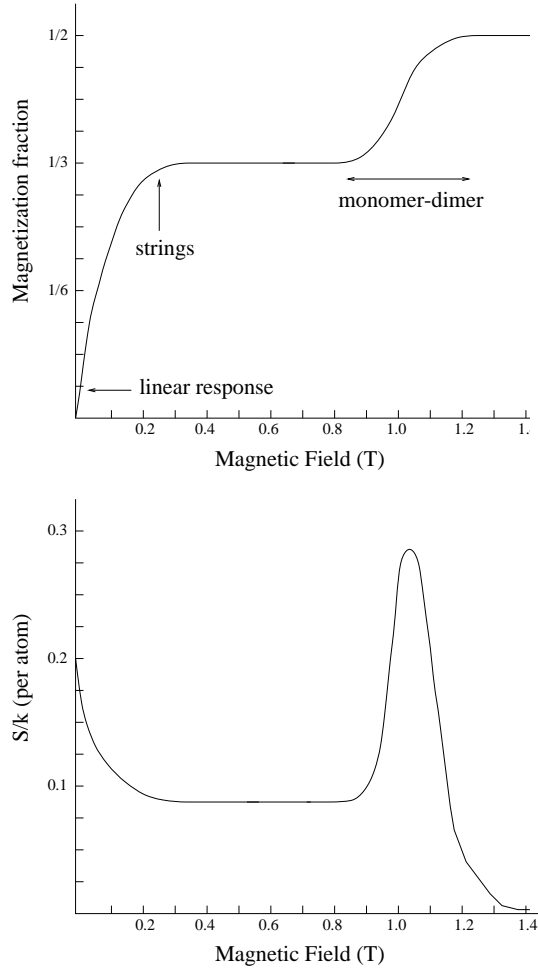
FIG. 1: Properties of spin-ice as the [111] magnetic field is varied. These curves are for illustration and do not show actual numerical or experimental data. We have indicated the regions where various analytic approaches discussed in the text apply.
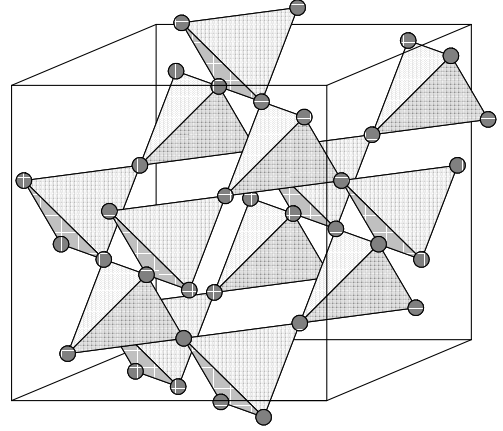
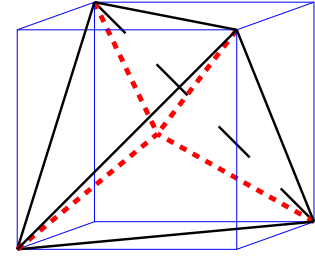FIG. 2: The pyrochlore lattice of corner-sharing tetrahedra.

FIG. 3: A single tetrahedron inscribed in a cube. The easy axes of the pyrochlore lattice (or $\langle 111 \rangle$ axes), $\hat{\mathbf{d}}_\kappa$, are indicated by the short-dashed lines.

II.   MODEL AND NOTATION

A general model of spin ice includes the single-ion anisotropy, the exchange interaction, and the dipolar interaction. In this work we use a simplified model[1] in which the long-range dipolar interaction is truncated beyond the nearest-neighbor spins. While the exchange interaction in spin ice compounds is antiferromagnetic, the effective interaction (exchange plus nearest-neighbor dipolar) is ferromagnetic. The Hamiltonian for unit-length spins $\mathbf{S}_i$ may be written as

$$
\begin{aligned}
H = {} & -J'_{\text{eff}} \sum_{<ij>} \mathbf{S}_i \cdot \mathbf{S}_j + E \sum_i \left(\hat{\mathbf{d}}_{\kappa(i)} \cdot \mathbf{S}_i \right)^2 \\
& + g\mu_B J \sum_i \mathbf{B} \cdot \mathbf{S}_i,
\end{aligned} \tag{2.1}
$$

where J'_{eff} is an effective exchange coupling. The second term is the easy axis anisotropy of strength $E < 0$,

$|E| \gtrsim 50K$, which is much larger than the exchange and dipolar interaction strengths. The unit vectors $\hat{\mathbf{d}}_{\kappa(i)}$ are the local easy axes of the pyrochlore lattice (see Fig. 2 and Fig. 3). The third term is the interaction with a magnetic field of strength B, $g\mu_B J$ being the magnetic moment of the spins. Both experiment and theory indicate that this simplified model is a good description of spin ice at moderate temperatures.

In our analysis, we take the single ion anisotropy to be infinite so the spins are constrained to lie along their local easy axes. In this limit, it is convenient to describe the system by the Ising pseudospins σ_i, where $\mathbf{S}_i = \sigma_i \hat{\mathbf{d}}_{\kappa(i)}$. The pseudospin $\sigma_i = +1(-1)$ if the physical spin points into (out of) its associated up-pointing tetrahedron. We may write an effective Hamiltonian for the pseudospins:

$$
H = J_{\text{eff}} \sum_{<ij>} \sigma_i \sigma_j - g\mu_B J \sum_i \mathbf{B} \cdot \hat{\mathbf{d}}_{\kappa(i)} \sigma_i, \tag{2.2}
$$

where $J_{\text{eff}} = J'_{\text{eff}}/3 > 0$.

III. THE LOW FIELD REGIME

At zero magnetic field and zero temperature, the ferro-magnetic interaction gives rise to an "ice rule" constraint: the pseudospins on each tetrahedron must sum to zero, $|\sum_\kappa \sigma_\kappa| = 0$. In terms of the physical spins, on each tetrahedron two will point inwards (towards the center) and two will point outwards (away from the center). The set of configurations satisfying the ice rule comprises the zero-field spin ice ground state manifold. At low magnetic fields (and low temperatures), the system will continue to obey the ice rule, though the magnetic field will favor certain states among those in the zero-field ground state manifold.

We have performed extensive Monte Carlo simulations of the low field regime, from zero-field up till the low field plateau termination, using a loop algorithm, which is discussed in Appendix A. Our algorithm probes only spin ice ground states (two spins in and two out on each tetrahedron) and is thus applicable at low temperatures $T \ll J_{\text{eff}}$ and low magnetic fields, where the density of monomer defects, which are responsible for the high field plateau termination, is low. The simulation is written in terms of a pyrochlore lattice with the conventional 16 site cubic unit cell (which contains four tetrahedra of each kind). The simulations have been done for systems with 16, 128, 432, 1024, 2000, 3456, 5488, 8192, and 16000 sites. For a system with 16000 sites, we perform 2.5×10^6 loop flips for equilibration and 5×10^7 for averaging. For other system sizes, we we perform 1×10^7 loop flips for equilibration and 2×10^8 for averaging. The simulated magnetization as a function of the magnetic field strength is shown in Fig. 4. The magnetization attains the plateau value at fields much larger than the temperature.
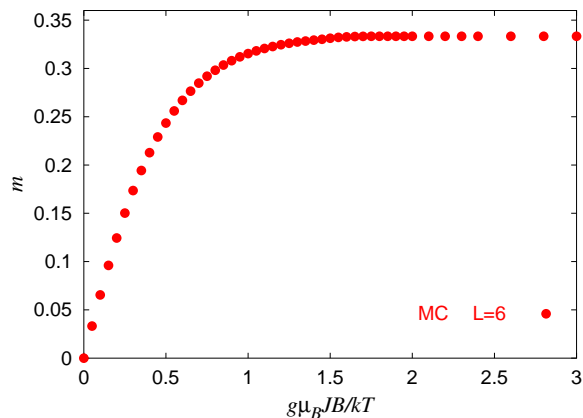

FIG. 4: The magnetization from Monte Carlo simulations.

A. The linear response regime

We may calculate the ground state entropy of spin ice at zero field by numerically integrating the first law of thermodynamics

$$dS = \frac{dU}{T} + \frac{m}{T}dh. \tag{3.1}$$

Noting that the magnetization is constant and equal to $-g\mu_B J/3$ per spin on the plateau and is zero at zero field, and that the value of the entropy on the plateau is $S/k_B = 0.080765$[10,11], we obtain for the entropy of spin ice, $S/k_B = 0.2051 \pm 0.0001$. Our value is very close to Pauling's estimate $S/k_B = 0.202733$ and is consistent with the most accurate current theoretical estimate $S/k_B = 0.20501 \pm 0.00005$.[15]

At zero field, we use the self-consistent Hartree approximation, which is known to give a quantitatively accurate approximation to the ground state correlations of spin ice.[13] This gives $\chi = 2(g\mu_B J)^2/3k_B T$ for spin ice. This compares well with our Monte Carlo result, $\chi = (0.66735 \pm 0.0003)(g\mu_B J)^2/k_B T$ for a system with 16000 sites.

B. String defects and their interactions

1. General description

Figure 2 presents the underlying pyrochlore lattice of spin ice and fig. 3 shows the [111] direction. It is convenient to visualize the pyrochlore lattice as a stack of alternating kagome and triangular planes, the [111] direction being the direction in which the planes are stacked. Each spin lies on a corner shared by an up-pointing and down-pointing tetrahedron.

If the [111] magnetic field is large enough, the spins in the triangular planes align with the field; the kagome planes decouple from one another; and the system is well described by a two-dimensional model. This describes spin ice on the plateau. At fields slightly lower than the plateau, excitations called string defects,[11] restore three-dimensionality and are responsible for the low field termination of the plateau.

To describe these defects, we consider the entropic benefit of relaxing the condition that the triangular planes are polarized. Suppose we flip a spin in some triangular layer. Then, by the ice rule constraint, we must also flip a spin in each of the two neighboring kagome layers (on the two tetrahedra that are sharing the first flipped spin). Flipping these kagome spins requires flipping spins in each of the two neighboring triangular layers, which requires flipping spins in the two next-nearest kagome layers and so on. The resulting "string defect" is an excitation that extends through the system. The energy cost, per kagome-triangle bilayer, of creating the string is $E_s = 8g\mu_B J B/3$. To estimate the entropy, we note that creating a string actually involves creating a pair of defects in each kagome plane. A "positive" defect connects the kagome plane to the kagome plane directly above it via a flipped spin in the intermediate triangular plane. Similarly, a "negative" defect connects the kagome plane

to the kagome plane directly below it. These two defects may be separated by flipping pairs of spins pointing in different directions on neighboring triangles of the kagome plane. The entropy in the kagome plane depends on this separation, which is the basis for the interaction between defects discussed below. Ignoring this correction, the positive defect may be placed anywhere in the plane (which fixes the position of the negative defect in the layer above). This implies that the entropy per bilayer is $S \sim \ln A$, where A is the area of a layer. This shows that for a given magnetic field, string defects are favored in a sufficiently large system. For a given system size, strings are favored at sufficiently low magnetic fields.

2. Interactions

For magnetic fields in the plateau region, the triangular spins are fixed while each kagome plane contains two up pseudospins ($\sigma = 1$) and one down pseudospin ($\sigma = -1$). This Ising model on the kagome lattice may be mapped onto the dimer model on the hexagonal lattice[10,11,12], where a down pseudospin corresponds to a dimer on the hexagonal lattice. In this language, a string defect appears as a pair of oppositely charged monomers.

As discussed in Ref. 11, a monomer-dimer covering may be described by assigning a height variable h_i to each site i of the triangular lattice dual to the hexagonal lattice on which the dimers lie. The heights are assigned as follows. Moving from a site to a nearest neighbor site by moving clockwise around an up- (down-) triangle will increase (decrease) the height by $+2$ (-2) if a dimer is crossed. If a dimer is not crossed, then the height will decrease (increase) by -1 (+1). According to these rules, traversing a closed loop in the dual lattice will result in a height difference of $+3$ (-3) if a positive (negative) monomer is enclosed and 0 otherwise. We note that the overall sign of the height assignments is a matter of convention and we may as well have chosen the h_i so that traversing a closed loop containing a positive (negative) monomer gave a height difference of -3.

In a coarse-grained description, the h_i are replaced by a real, continuum field $h(\vec{r})$ and as discussed in Ref. 11, the entropy associated with a height field $h(\vec{r})$ is given to lowest order ingredients by:

$$S = \int d^2r \frac{K}{2} |\nabla h|^2 \qquad (3.2)$$

where $K = \frac{\pi}{9}$ for the honeycomb lattice.[16] The height field has the property:

$$\oint_C \nabla h \cdot d\vec{r} = 3 \int_S d^2r \sigma(\vec{r}) \qquad (3.3)$$

where $\sigma(\vec{r})$ is the monomer charge density and S is the region enclosed by the loop C. We may proceed by analogy with the 2d XY model[17] and divide h into "dimer"

(spin-wave) and "monomer" (vortex) contributions. A standard calculation[18] gives the entropy of the monomer piece:

$$
\begin{aligned}
S_m &= \frac{9K}{4\pi} \int \int d^2r d^2r' \sigma(\vec{r})\sigma(\vec{r'}) \left(-\ln \frac{|\vec{r}-\vec{r'}|}{\tau} \right) \\
&= \frac{1}{2} \int \int d^2r d^2r' \sigma(\vec{r})\sigma(\vec{r'}) \left(-\kappa \ln \frac{|\vec{r}-\vec{r'}|}{\tau} \right)
\end{aligned}
$$
$$(3.4)$$

where $\kappa = 1/2$ and τ is a hard-core radius comparable to the lattice spacing. This shows that the entropic interaction between two defects separated by distance r is given by $p_1 p_2 V(|\vec{r_1} - \vec{r_2}|)$ where p_i is +1 (-1) for a positive (negative) defect and $V(R) = -\kappa \ln(R/\tau)$.

3. Mean field calculation

If the number of defects is fairly large, we may expect the interaction to be sufficiently screened to justify the use of variational mean field theory.[19] We will investigate the in-plane and out-of-plane correlations for the defects.

We consider a layered system of two-dimensional planes (indexed by the label k which ranges from $-K$ to K) where each plane contains N positive and N negative defects (which we refer to as charges) that interact logarithmically. The string constraint requires that each positive charge in layer k is rigidly connected to a negative charge in the layer $k + 1$. We impose a periodic boundary condition to connect the positive charges in the Kth layer to the negative charges in the $-K$th layer.

We formally impose the constraint by writing the "Hamiltonian" in terms of positive charges alone. The planes are stacked in the z-direction. Let x_i^k be the in-plane position of the ith positive charge in the kth layer. In absence of external fields, the entropy of a particular configuration of N defects is given by:

$$H = \sum_{k=-K}^{K} \left(\sum_{i \neq j}^{N} V(|x_i^k - x_j^k|) - \sum_{i,j}^{N} V(|x_i^k - x_j^{k+1}|) \right) \quad (3.5)$$

Here $V(R) = -\kappa \ln(R/\tau)$, where τ is a hard-core radius defining the minimum separation between two charges and $\kappa = 1/2$. The first term corresponds to the repulsion of positive charges within the same layer. The absence of a factor of $\frac{1}{2}$ in front of this term is due to the string constraint: bringing two positive charges in the same plane close together also involves bringing together their negative partners in the plane above. In terms of our positive charge formulation, this means the repulsion is twice as large. The second term is the interlayer interaction. Physically, a positive charge in layer k has a negative partner in the layer $k+1$ which attracts the positive charges in layer $k+1$. In terms of our positive charge formulation, charges repel charges in the same plane but attract charges in nearest neighbor planes.

We assume a variational mean field density of the form:

$$\rho(x_1^{-K}, ..., x_i^k, ..., x_N^K) = \prod_{k=-K}^{K} \prod_{i=1}^{N} \frac{\rho^k(x_i^k)}{N} \qquad (3.6)$$

which asserts that all particles in a given layer k have the same probability density $\rho^k(x)/N$, but the density may vary from layer to layer. We also need the normalizing condition:

$$\int_A d^2 x \rho^k(x) = N \qquad (3.7)$$

This trial function implies a variational entropy functional:

$$
\begin{aligned}
S_{\rho,N} = & \sum_{k=-K}^{K} \left(-\frac{1}{2} \int \int d^2 x d^2 x' (\rho^k(x) - \rho^{k+1}(x)) \right. \\
& \times \ (\rho^k(x') - \rho^{k+1}(x'))V(|x - x'|) \\
& \left. - \int d^2 x \rho^k(x) \ln(\frac{\rho^k(x)}{N}) \right)
\end{aligned}
\qquad (3.8)
$$

This functional is maximized when the density is uniform $\rho^k(x) = \frac{N}{A}$ which gives $S_{\rho,N} = (2K+1)N \ln A$. To investigate the linear response of the system, we may apply a perturbing potential to the objects in the $k = 0$ plane. In particular, we consider the effect on the density of placing a positive charge at the origin of the plane. The details are given in Ref. 18 but we may quote the result:

$$
\begin{aligned}
\delta\rho(\frac{x}{\xi_\parallel}, k) = & \frac{1}{4\pi^2 \xi_\parallel^2} \\
\times & \int \frac{d^2 s \left[s^2(s^2 + 2) \right]^{-1/2} e^{is \cdot (\frac{x}{\xi_\parallel})}}{\left[1 + s^2 + 2\sqrt{s^2(s^2+2)} \right] \left[1 + s^2 + \sqrt{s^2(s^2+2)} \right]^{k-1}}
\end{aligned}
\qquad (3.9)
$$

where the in-plane length scale is given by $\xi_\parallel = \left(\frac{A}{4\pi\kappa N} \right)^{1/2}$. We note first that this expression diverges at small x for $k = 0$, which is not surprising because the assumption of a linear response would be not be valid so close to the perturbing charge. The expression would be valid at larger k and an interesting feature is that when $x = \xi_\parallel$, the decay in the z-direction does not depend on any physical parameters, i.e. there is no length scale in the z direction. We will return to this point in the next section.

To connect with our physical problem, we note that at a given temperature, we will have an expected value of defects which may be calculated from the partition function:

$$\mathcal{Z} = e^{-\beta \mathcal{A}} = \sum_N \frac{y^{(2K+1)N}}{(N!)^{2K+1}} e^{S_N} \qquad (3.10)$$

where S_N is the entropy of having N defects and $y = e^{-E_s/k_B T}$ is the fugacity of a positive defect (y^{2K+1} is the fugacity of a "string"). In mean field, we may replace S_N by $S_{\rho,N} = (2K+1)N \ln A$. From this, we may show[18] that $< N > \sim yA$ and using our earlier expression, we find that:

$$\xi_{\parallel, MF}^2 \sim \exp(8g\mu_B JB/3k_B T) \qquad (3.11)$$

4. RG calculation

When the gas of defects is fairly dilute, we may expect that the screening is not effective enough to justify a mean field treatment. In this section, we account for fluctuations by making a real space renormalization group calculation using methods similar to the Kosterlitz treatment of the 2d Coulomb gas.[17,20]

The dynamical objects described by Hamiltonian 3.5 are dipoles of length 1. We need to generalize this model in order to do an RG calculation. The generalization that we consider is allowing for dipoles of arbitrary length. An "l-dipole" is an object where the negative charge lies directly l planes above its positive partner. While the original problem involved just the coupling of nearest neighbor planes, our generalized model involves all possible couplings. Associated with each l-dipole is a fugacity $y_l/2\pi$ (the 2π is for convenience). The grand partition function for the system may be written as:

$$\mathcal{Z} = \sum_{\{N_{k,l}\}} \left[\prod_{k,l} \frac{(y_l/2\pi)^{N_{,l}}}{(N_{k,l})!} \right] Z[\{N_{k,l}\}] \qquad (3.12)$$

where $N_{k,l}$ denotes the number of l-dipoles in layer k; $N_{,l}$ is the number of l-dipoles in the system; and N_k is the number of dipoles (of any length) that have their positive ends in layer k. The sum is over all particle number configurations $\{N_{k,l}\}$ that satisfy the charge neutrality constraint in each plane: $N_k = \sum_l N_{k-l,l}$. The canonical partition function corresponding to a given dipole distribution $\{N_{k,l}\}$ is:

$$
\begin{aligned}
Z[\{N_{k,l}\}] = & \int_{\Omega_\tau} \prod_{k,i} \left(\frac{d^2 x_{k,i}^{(1)}}{\tau^2} \frac{d^2 x_{k,i}^{(2)}}{\tau^2} \delta\left(\frac{x_{k,i}^{(1)} - x_{k,i}^{(2)}}{\tau} \right) \right) \\
& \times \ \exp\left[-H(\{N_{k,l}\}) \right]
\end{aligned}
\qquad (3.13)
$$

$H(\{N_{k,l}\})$ is the Hamiltonian (actually an entropy) corresponding to the dipole distribution $\{N_{k,l}\}$. The coordinate $x_{k,i}^{(1)}$ is the planar coordinate of the ith positive charge of layer k and $x_{k,i}^{(2)}$ is the planar coordinate of its negative partner which lives in layer $k + l(i)$, $l(i)$ being the length of the dipole being described. The string constraint is imposed by the delta function, where we use the normalization $\int_{\mathbf{R}^2} \frac{d^2 x}{\tau^2} \delta(\frac{x}{\tau}) = 1$. The product is over all positive charges in all layers. The integration is over the space Ω_τ. This is defined to be the set of all possible spatial configurations of the dipole distribution $\{N_{k,l}\}$

that respect the hard-core constraint: no two charges in a given plane may be closer than distance τ.

Our procedure is an extension of the treatment in Refs. 17,20. The first part of an RG procedure normally involves integrating over the high momentum modes of the system. In our problem, these correspond to those configurations where in some plane, we have a pair of charges separated by a distance between τ and $\tau+d\tau$. We assume a dilute system so only oppositely charged pairs are considered and also the distance between the members of a pair is taken to be much smaller than the distance from the pair to another charge. The basic coarse-graining step in our RG transformation is illustrated in fig. 5.
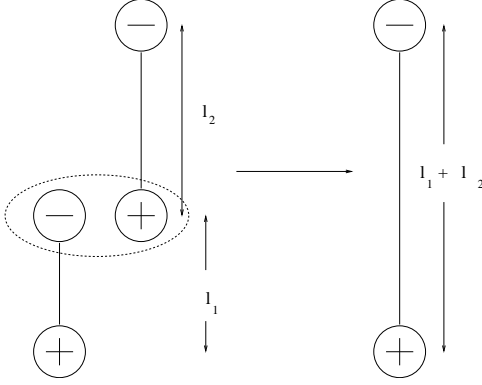

FIG. 5: The basic coarse-graining step in our RG transformation.

Suppose a particular state involves pairing the negative end of an l_1-dipole in layer k with the positive end of an l_2-dipole in layer $k+l_1$. Viewed at long length scales, we effectively have an (l_1+l_2)-dipole in layer k. We will find that integrating over all possible pairings gives a zeroeth order term (which just involves replacing Ω_τ with $\Omega_{\tau+d\tau}$) and a number of correction terms of order $d\tau$ where two short dipoles were destroyed and replaced by a longer dipole. Since the procedure respects the charge neutrality constraint, these correction terms will combine with other terms in the grand partition sum. The second step involves rescaling lengths so that the high momentum cutoff, in the new variable, is the same as before. The aim is to see how the fugacities and couplings change as we run this procedure.

Details of the calculation are given in Appendix B. Here we give the resulting flow equations:

$$\frac{dy_1}{dt} = (2-\kappa)y_1 \qquad (3.14)$$

$$\frac{dy_l}{dt} = (2-\kappa)y_l + \sum_{m=1}^{l-1} y_m y_{l-m} \qquad (3.15)$$

$$\frac{d\kappa}{dt} = 0 \qquad (3.16)$$

where $t = \ln\tau$. One notable feature is that the coupling does not change with the flow, in contrast with the 2d

Coulomb gas where the coupling does vary (albeit at second order in the fugacity). This indicates that strings are stiffer objects than charges. Another observation is that for the initial conditions of our physical problem, namely that $y_1(0) = y_0 = 2\pi e^{-E_s/k_b T}$ and $y_l(0) = 0$ for $l > 1$, the flow equations have an exact solution:

$$y_l = y_0\tau^{2-\kappa}\left[\left(\frac{y_0}{2-\kappa}\right)(\tau^{2-\kappa}-1)\right]^{l-1} \qquad (3.17)$$

Our RG is valid as long as the corrections to the fugacities are small, meaning that the derivatives dy_l/dt should be bounded. If we look at the above result, Eq. 3.17, we see that when the term in brackets is greater than 1, y_l diverges with l. Therefore, a critical length, which we interpret as an in-plane correlation length, is defined by when the term in brackets equals 1:

$$\frac{y_0}{2-\kappa}(\xi_{\parallel,RG}^{2-\kappa}-1) = 1 \qquad (3.18)$$

Substituting earlier expressions and noting that for our system, $\kappa = 1/2$, we find that:

$$\ln\xi_{\parallel,RG}^2 = \frac{32g\mu_B JB}{9k_B T}\left(1 + \frac{\ln(e^{-E_s/k_B T}+2-\kappa)}{E_s/k_B T}\right)$$
$$\xi_{\parallel,RG}^2 \sim \exp(32g\mu_B JB/9k_B T) \qquad (3.19)$$

for the fields and temperatures of interest. This value is the same as that predicted in Ref. 11 using a free energy argument. For $\tau < \xi_{\parallel,RG}$, y_l decreases with l which means that states with long dipoles are less probable than states with short dipoles. If $\tau > \xi_{\parallel,RG}$, y_l diverges with l which suggests that longer dipoles are favored, but, as mentioned above, the RG procedure is no longer valid in this regime. We note that when $\tau = \xi_{\parallel,RG}$, y_l is independent of l so that, as in the mean field calculation discussed above, there is no discernible length scale in the z direction.

If $\tau < \xi_{\parallel,RG}$, then we may consider an out-of-plane length scale, which we define nominally as the value of $l = l_\tau$ for which $y_l/y_1 = 1/e$.

$$l_\tau = 1 + \frac{1}{\ln\left(\frac{\xi_{\parallel,RG}^{3/2}-1}{\tau^{3/2}-1}\right)} \qquad (3.20)$$

We may interpret l_τ as the typical length of a string segment that is captured by a tube of diameter τ (where a tube need not be straight).

5. Comparison with simulation

In Fig. 6, we show the magnetization as a function of the magnetic field strength on a log-log scale. Our algorithm allows us to simulate spin ice in a [111] magnetic field with very high accuracy.

The magnetization should scale with the average density of defects, which in turn should scale like the inverse
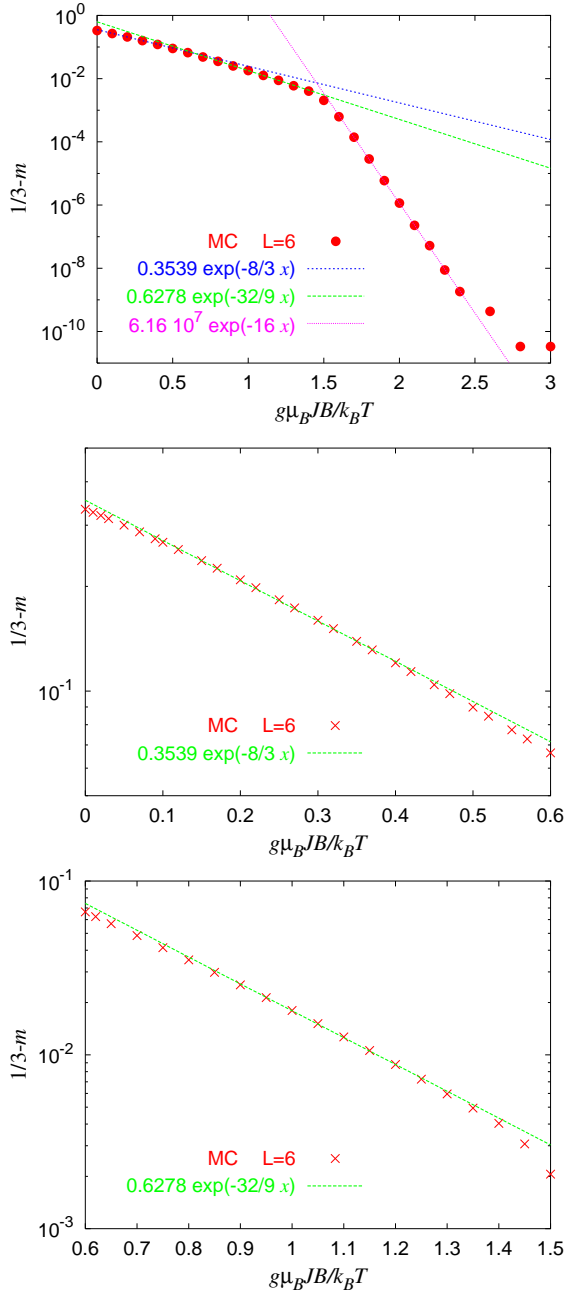
FIG. 6: The crossover between exponents.

one another which suggests that a mean field treatment may be reasonably accurate. At higher fields, the gas of defects is more dilute so an RG treatment would be required.

The high field crossover is a finite-size effect since the position of a crossover between exponents is system size dependent and the corresponding exponent is also system size dependent, getting steeper with increasing system size. The finite-size behavior may be explained as follows. At high magnetic fields, there are a small number of string defects in the system. The magnetization and the energy of one string defect in a system of size L are $-4Lg\mu_B J/3$ and $4Lg\mu_B JB/3$ respectively. The energy cost grows linearly with system size and, as mentioned above, the defects are favored solely due to their entropic contribution to the free energy. At sufficiently high magnetic fields, a given system will be too small to provide the entropy to balance the energy cost of a string. This will occur when the magnetization per spin reaches the magnetization of a system with one string defect:

$$m = \left[1/3 - 2(4L/3)/(16L^3)\right] g\mu_B J$$
$$= \left[1/3 - 1/(6L^2)\right] g\mu_B J. \qquad (3.21)$$

In this case, the statistical weight of a single string defect will be a Boltzmann factor $\exp(-8Lg\mu_B JB/3k_B T)$ and the magnetization will equal $\left[1/3 - C\exp(-8Lg\mu_B JB/3k_B T)\right] g\mu_B J$, where C is some constant. The crossover between different regimes occurs when the magnetization reaches (3.21). We have good agreement with the $8L/3$ behavior for a variety of system sizes, including $L = 6$ which is shown in figure 6.

IV. THE HIGH FIELD REGIME

On the plateau, the magnetization of the triangular sublattice is saturated and we may consider each kagome plane separately. Thus, the 3-dimensional model may be mapped onto a 2-dimensional one. Whereas the spins in the triangular sublattice are fixed, the physics in the kagome planes remains non-trivial. Each triangle on the kagome plane contains two up pseudospins ($\sigma = 1$) and one down pseudospin ($\sigma = -1$). This Ising model on the kagome lattice may be mapped onto the dimer model on the hexagonal lattice,[10,11,12] in which a down pseudospin corresponds to a dimer on the hexagonal lattice. The model retains an extensive ground state entropy, $S/k_B = 0.080765$.

If we flip a down (pseudo)spin it violates the ice rule. This corresponds to breaking a dimer into two monomers. As with string defects, these monomers may be separated and move freely on the lattice. The energy cost for creating two monomers is $2\mathcal{E} = 4J_{\text{eff}} - 2g\mu_B JB/3$. This energy vanishes at a critical field $B_c = 6J_{\text{eff}}/(g\mu_B J)$. At higher fields the monomers proliferate leading to complete saturation and an ordered state with zero entropy.

square of the in-plane correlation length. As shown in this figure, the data at low fields are well fit by the exponent $8/3$ obtained in the mean field calculation discussed earlier. At somewhat higher fields, the data are well fit by the exponent $32/9$, obtained by the RG calculation discussed earlier and also in Ref. 11 by looking at the entropic contribution to the free energy. At high fields, the exponent of $8L/3$ (=16 for L=6 (sites), as was the case in the simulations) characterizes a regime where finite-size effects are important, as discussed below.

The low field crossover makes qualitative sense in that at low fields, there will be many defects which screen

The physics near the transition may be described by the following Hamiltonian which acts on the kagome lattice:

$$\frac{H}{T} = \sum_{\langle ij \rangle} K_{ij} s_i s_j - h \sum_i s_i, \qquad (4.1)$$

where the sum is over all nearest neighbors; s_i are classical Ising spins taking values $+1$ and -1; h is the strength of a fictitious magnetic field; and $K_{++} = 0$, $K_{+-} = K_{-+} = K = [g\mu_B JB/6 - J_{\text{eff}}]/T$, and $K_{--} = \infty$. The coupling constants imply that each triangle of the kagome lattice contains at most one down pseudospin and that down spins cost energy (positive or negative dependent on the magnetic field strength).
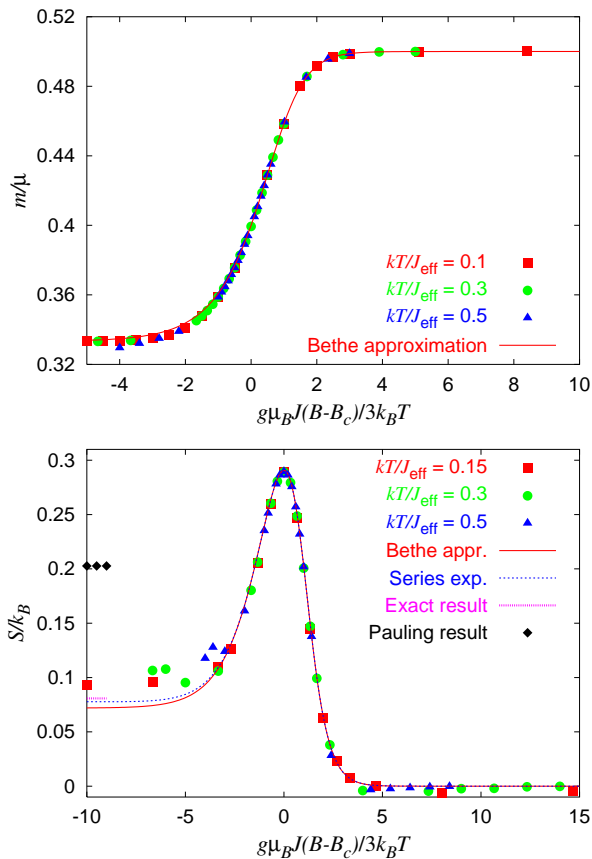

FIG. 7: The magnetization (top) and the entropy (bottom) around the transition between the plateaux. The simple Bethe approximation is compared to the Monte Carlo results. The exact result for the entropy at zero monomer density and Pauling's estimate for the entropy at zero magnetic field are shown for reference. The series expansion contains the results from Ref. 14 on the monomer-dimer model.

We may calculate the magnetization and entropy using the simple Bethe approximation. Details are given in Refs. 14,21 but we may quote the results:

$$m = \frac{1}{2}\frac{1}{1+x^2} \qquad (4.2)$$

$$S = -\frac{3xz\ln z}{2+6xz} + \frac{1}{4}\ln\frac{2z^3}{x^2(3z-x)}, \qquad (4.3)$$

where $x = 2z/(1 + \sqrt{1 + 8z^2})$ and $z = \exp(-2K)$.

In Fig. 7, we compare these expressions with a Monte Carlo simulation. The simulation is of a kagome lattice with 16x16 up-triangles (768 total spins). The standard single spin-flip Metropolis algorithm was used, which may explain the inaccuracy in the simulated entropy at low fields, where a more clever scheme may be needed to sample the degenerate manifold. The entropy was computed, for a given field, by integrating from high temperatures (where $S/k_B = (3/4)\ln 2$ per atom) to low temperatures.

We find that the simple Bethe approximation is accurate for moderate and high monomer densities (higher fields) but does not work so well at low monomer density (lower fields). As the Bethe approximation does not account for long cycles on the lattice, the approximation should indeed break down when the correlation length is large (monomer density is small). We note that the correlation length is infinite at zero monomer density since the dimer model on the hexagonal lattice is critical.

In a higher-order series expansion, one may account for some corrections to the Bethe approximation.[14] As seen in the figure, the corrections are almost indiscernible for the magnetization. For the entropy, the corrections give better agreement at the low monomer density and are negligible at high monomer densities.

There is a giant peak in the entropy at the transition point, $S/k_B = 1/4\ln(16/5) \approx 0.291$, which exceeds even the zero field entropy. The peak is due to the crossing of an extensive number of energy levels which have macroscopic entropies. For $B = B_c$, the energies of states corresponding to different numbers of monomer defects are equal since the monomer and dimer weights are, by definition, equal at the critical field. There are an extensive number of states corresponding to a given number of monomers (below saturation). The highly degenerate ground state manifold explains the large spike in the entropy.

V. CROSSING POINTS

The theory described in the previous section implies that the curves of magnetisation versus field, plotted for different temperatures, will display a crossing point. This arises simply because the partition function depends on magnetic field and temperature effectively only through the combination $(B - B_c)/T$. Thus, when plotted as a function of $B - B_c$, the curves coincide only at the point $B = B_c$. At this point, the Bethe approximation gives a value for the magnetisation of $m = 0.4g\mu_B J$, see Eq. 4.2.

In addition, we expect a crossing point at low fields, due the interplay of string and monomer defects. Indeed, where the plateau is well-formed, the string density is $n_s \sim \exp(-32g\mu_B JB/9k_b T)$ and the monomer density is $n_m \sim \exp(-8\mathcal{E}_m/7k_B T)$, where $\mathcal{E} = g\mu_B J(B_c - B)/3$ is the energy of creating one monomer. The crossing point occurs when $n_s = n_b$. With logarithmic accuracy, we can

write

$$\frac{32g\mu_B JB}{9k_b T} = \frac{8g\mu_B J(B - B_c)}{21k_B T}. \qquad (5.1)$$

Thus the crossing point lies at $B^\star = 3B_c/31$.

VI.   RELATION TO EXPERIMENT AND OTHER THEORIES

Our model gives a description of the high field transition that is qualitatively consistent with experiment for a range of temperatures[4]. In particular, a peak in the entropy has been observed close to the high-field termination of the plateau (Fig. 9 in Ref. 4). As this feature was taken to be an experimental artefact, it was not analyzed in detail in that work. However, it appears that its height is rather smaller than the one we find here, although the number of data points is not enough to determine the center of the peak or its height.

However, recent experiments[22] on the spin ice compound $Dy_2Ti_2O_7$ have indicated that at low temperatures, the high field transition becomes first order. In Ref. 22, the onset of first order behavior was found to occur for temperatures lower than a critical temperature of $T_c \sim 0.36K$ ($\sim 0.327J_{eff,Dy}/k_B$). Figure 7 shows that our predicted curves remain continuous even at temperatures below this observed T_c.

A likely reason for the discrepancy is the long range nature of the dipolar interaction, which we approximated as a nearest neighbor Ising model. The simplest way to account for these interactions is to model the ignored interaction terms as giving rise to a magnetic field proportional to the magnetization. By assuming the magnetization M, as a function of the effective field $B + \alpha M$, has the same functional form as given in figure 7, we may self-consistently determine M for a given B. Using α as a free parameter, we find that this simple model predicts the onset of first order behavior, at the experimentally observed critical field B_c, only for temperatures in the millikelvin range. To obtain a higher numerical T_c requires a larger α, which causes a lower numerical B_c. To get the numerical T_c to match experiment requires an α so large that our numerical B_c is "negative" (in the sense of artificially extending the $M = 1/3$ line of figure 7 for the purpose of a spline fit). It seems that a more careful treatment of the dipolar interaction is required in order to explain the recent experimental results. Also, we have not considered the impact of the slowdown of the dynamics which is observed at low temperature.[23]

As for the crossing points mentioned above, the high-field one does indeed appear to be present in the experimental data[3,22] in the appropriate temperature range. The experimental value of the magnetization at the crossing point is about $m = 0.38g\mu_B J$, reasonably close to the theoretical value $m = 0.4g\mu_B J$. By contrast, a crossing point at small fields is harder to make out, and an approximate estimate of its location gives $B^\star = 0.35B_c$, in disagreement with the theoretical $B^\star = 3B_c/31$.

VII.   ENTROPY SPIKE AND MAGNETOCALORICS

Fig. 7 shows a stark contrast between the behavior of magnetization and entropy as the field strength is increased. Whereas the magnetization increases monotonically going from one plateau to the other, the entropy displays a strong (but smooth) non-monotonicity.

One question which naturally arises is whether such an entropy peak exists more generally between two magnetization plateaus – what is the crucial ingredient for the existence of the spike? The sectors with different magnetizations are degenerate because not only do the monomer defects not cost any energy at the degeneracy point, but they also do not interact. Such a situation has in fact been observed already in a much more familiar frustrated model, namely the triangular Ising antiferromagnet in a longitudinal field. Here, there is a (non-degenerate) low-field plateau with magnetization of $1/3$, in addition to the usual saturated high-field plateau. These two are separated by a degeneracy point where 'up-up-up' and 'up-up-down' triangles are degenerate.[24] The statistical mechanics of that point is described by the hard-hexagon model,[25] the entropy of which is extensive. A similar phenomenon – a magnetization plateau bounded by two entropy spikes – also appears in the case of an effectively 1d helimagnet.[26]

In classical Ising models, such a degeneracy seems not so surprising as the allowed energies are naturally discrete. However, a similar situation can arise even in bona-fide Heisenberg models. This follows from the result by Richter *et al.*,[27] who demonstrated that near saturation, on a range of frustrated lattices (including the kagome), localized spin-$1/2$ excitations exist. As one sweeps the magnetic field from saturation downwards, one would therefore also expect an entropy spike in those models. A numerical study testing this assertion is in progress.[28]

Cooling by adiabatic (de)magnetization

At low temperatures, near the degeneracy point, the partition function depends on magnetic field and temperature effectively only through the combination $(B - B_c)/T$. One may thus argue that the spike may be used to effect cooling by adiabatic demagnetization[29] in exactly the same way one may use paramagnets – analogous constraints limit the application in either case.

There are two features which may be worth pointing out at this point. Both follow from the fact that – unlike in the case of a paramagnet – $B_c \neq 0$. Firstly, maximal cooling occurs at a finite field, namely around B_c. This phenomenon may therefore be useful to effect cooling for a magnet in a field, with the restriction that B_c, for a

given spin ice compound, is not tunable. Secondly, if B approaches B_c from below, one can in fact obtain "cooling by adiabatic magnetization", as entropy and magnetization grow together in this regime.

VIII.   CONCLUSIONS

In this paper, we have analyzed in detail the magnetization curve of nearest-neighbor spin ice in a [111] magnetic field. The basic ingredient which makes this system particularly interesting is that a uniform field can be used to couple to the Ising pseudospins as a staggered field.[30,31] This amounts to the possibility of applying fields which would have appeared to be rather unnatural in the formulation of a simple Ising model (without the detour via spin ice) on the pyrochlore lattice.

As a result, one observes an attractively rich behavior. Perhaps the most salient is the dimensional reduction from pyrochlore to kagome under the application of an external field. The restoration of three-dimensionality upon weakening the field goes along with the one-dimensional string defects. We hope that the extension developed here of Kosterlitz's RG treatment to such extended defects might be of more general use.

A particularly attractive feature of the monomer-dimer model we have obtained here lies in the fact that the relative monomer and dimer fugacities in the low-temperature ($T \ll J_{\text{eff}}$) regime are given by simple Boltzman weights of Zeeman energies. They are thus straightforwardly tunable by changing the strength of the applied field. In particular, anisotropic fugacities can be obtained by tilting the field, and they therefore do not require an actual manipulation (such as an application of anisotropic stress) of the two-dimensional layer.

As discussed previously in Ref.[11] the price for our ability to analyze the model in such detail has been the omission of the long-range nature of the dipolar interaction. A truncation of the interaction at only the nearest-neighbor distance would seem a rather drastic step; an expectation of quantitative agreement between experiment and the nearest-neighbor model will in general likely be misplaced. However, as we argue in a different context, it turns out that, in an intermediate temperature regime, this is not entirely unreasonable.[13] This observation might lie at the basis of the fact that the measured dipolar ice entropy agrees so well with Pauling's estimate. Our 'prediction' of the entropy peak between the intermediate and saturated plateaux bears witness to the promise of our approach to unearth at least some qualitative features of interest.

Acknowledgements

APPENDIX A: THE CLUSTER ALGORITHM

We use a loop algorithm to simulate spin ice at low fields. The algorithm probes only the spin ice ground state manifold and therefore can work only at low temperatures and low magnetic fields. All attempted loop flips are accepted in our algorithm.

The algorithm works as follows. To construct a loop, we, first, pick at random a tetrahedron of fixed orientation (and mark it as a first tetrahedron in a loop), then we pick with probability 1/2 a spin direction (in or out of a tetrahedron) and pick a first spin in a loop using the following rules. If both spins with the chosen direction are on the kagome sublattice then we pick the spin with a probability 1/2, which is independent of the spin orientation. If one spin is on the triangular sublattice and another is on the kagome sublattice then we pick the spin with probability that depends on the spin orientation. Namely, if the spin on the triangular sublattice is out of the tetrahedron (along the magnetic field), we pick the spin on the kagome or triangular sublattices with respective probabilities

$$p_1 = \frac{1}{1+g}, \tag{A1}$$

and

$$p_2 = \frac{g}{1+g} \tag{A2}$$

where g will be fixed by the detailed balance condition, see below, and $p_1 + p_2 = 1$. If the spin on the triangular sublattice points into the tetrahedron, we pick the spin on the kagome or triangular sublattices with probabilities p_2 and p_1 respectively. Then we flip the chosen spin thus introducing two defects in the tetrahedra that share the spin.

After choosing the first spin, we move to the neighboring tetrahedron with a defect. The next tetrahedron has two spins with the opposite orientation. We flip one of these two spins adding it to the loop using the same prescription as we used to pick the first spin. Thus we move the defect to another tetrahedron. Then we repeat this procedure iteratively moving one of the two defects through the lattice until we encounter the other defect in the first tetrahedron – the two defects will annihilate and the loop will be closed. Since we add spins to the loop with alternating signs – two spins with opposite orientation from each tetrahedron we traverse, the ice rule is not violated.

The algorithm is ergodic since any pair of different configurations differ by spins on closed loops only. They can always be connected by flipping these loops.

Let us sketch the proof of the detailed balance condition. Suppose that we have flipped some loop. In order to prove detailed balance, the first site in a loop that returns us to the original configuration must be the first site in the original loop and the reversed loop must be constructed in the reverse direction. We can prove the detailed balance condition locally, i.e. for all short sequences of the loop, see Fig. 8 and Fig. 9. It is easy to check that most of these sequences are trivial, i.e. they have equal energies before and after spin flip and equal probabilities to go from one to another configuration. An
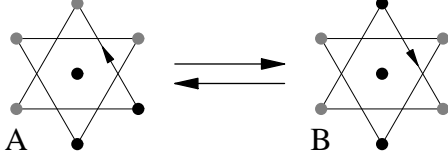

FIG. 8: Configurations A and B. Tetrahedra are shown on top of each other. Small arrows indicate a short sequence of a loop. Up and down spins are denoted by black and grey dots.

example of such a simple sequence is shown in Fig. 8. The probability of going from configuration A to configuration B is equal to the probability of going from B to A (equal to $1/2$). In order to prove the detailed balance condition, we only need to consider the energies of single spins that are the second spins in the sequences (the energies of the first spins in the sequences are taken into account in the previous step). These spins have the same energies. Thus the detailed balance condition is satisfied trivially. An example of a nontrivial sequence is shown in Fig. 9. The energies of configurations A and B' are different there. We have to prove the detailed balance
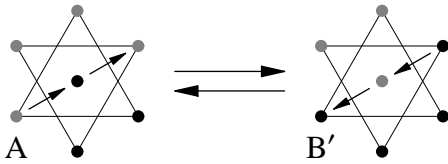

FIG. 9: Configurations A and B'. Tetrahedra are shown on top of each other. Small arrows indicate a short sequence of a loop. Up and down spins are denoted by black and grey dots.

condition

$$P(A \to B)/P(A \leftarrow B') = P(B')/P(A) \qquad (A3)$$

The right hand side in (A3) is just a ratio of Boltzmann weights and is equal to $\exp(8h/3)$, where $h = g\mu_B JB/k_B T$, since the energy of configuration A (the energy of the second and third spins in the sequence) is $4hk_B T/3$, and the energy of configuration B' (the energy of the second and third spins in the sequence) is $-4hk_B T/3$. According to our algorithm, the probability of going from configuration A to configuration B' is

$P(A \to B') = p_1/2$ and the reverse probability of going from B' to A is $P(A \leftarrow B') = p_2/2$. We have from (A3)

$$g = \frac{p_2}{p_1} = \exp(-8h/3). \qquad (A4)$$

Therefore if we choose p_1 and p_2 as

$$p_1 = \frac{1}{1 + e^{-8h/3}}, \qquad (A5)$$

and

$$p_2 = \frac{e^{-8h/3}}{1 + e^{-8h/3}} \qquad (A6)$$

then the detailed balance condition is fulfilled.

APPENDIX B: RG CALCULATION

We introduce the abbreviation:

$$d\Omega_\tau = \prod_{k,i \in I_k} \left(\frac{d^2 x_{k,i}^{(1)}}{\tau^2} \frac{d^2 x_{k,i}^{(2)}}{\tau^2} \delta\left(\frac{x_{k,i}^{(1)} - x_{k,i}^{(2)}}{\tau} \right) \right) \qquad (B1)$$

in terms of which the canonical partition function for a given dipolar distribution $\{N_{k,l}\}$ may be written: $Z(\{N_{k,l}\}, \tau) = \int_{\Omega_\tau} d\Omega_\tau \exp(-H)$. Our RG calculation has two steps. The first step is integrating over short length scales, i.e. those states where at least one pair of charges is separated by a distance between τ and $\tau + d\tau$. The second step is to rescale variables to restore the short distance cutoff. When we carry out the first step, the result is a zeroth order term and a correction of order $d\tau$:

$$Z(\{N_{k,l}\}, \tau) = \int_{\Omega_{\tau+d\tau}} d\Omega_\tau \exp(-H) + \sum_{k,l,m,i,j} I_{klmij} \qquad (B2)$$

where I_{klmij} is the contribution of the configuration that has the negative end of the ith m-dipole of layer k paired with the positive end of the jth $(l-m)$-dipole of layer $k + m$. The sum over k is over all planes; the sum over l is over all dipole lengths up to the number of planes; and the sum over m is from 1 to $l - 1$. The form of this term is given by:

$$\begin{aligned} I_{klmij} = & \int_{\Omega'_{\tau+d\tau}} d\Omega'_\tau e^{-H'} \int_A \frac{d^2 x_i^{(2)}}{\tau^2} \delta\left(\frac{x_i^{(1)} - x_i^{(2)}}{\tau} \right) \\ \times & \int_{d(x_i^{(2)},\tau)} \frac{d^2 x_j^{(1)}}{\tau^2} \delta\left(\frac{x_j^{(1)} - x_j^{(2)}}{\tau} \right) e^{-H(x_i^{(2)}, x_j^{(1)})} \end{aligned} \qquad (B3)$$

The region of integration of the positive charge $x_j^{(1)}$ is an annulus of radius τ and thickness $d\tau$ centered on the negative charge $x_i^{(2)}$. This region is denoted by $d(x_i^{(2)}, \tau)$. The position of this negative charge (and hence the pair) is integrated over the entire area A. Strictly speaking,

$x_i^{(2)}$ would have to avoid the hard cores of all of the other charges but this introduces an error of order $(d\tau)^2$. $\Omega'_{\tau+d\tau}$ is the space of configurations of the rest of the charges in which the charges are separated from each other by a distance of at least $\tau + d\tau$. $H(x_i^{(2)}, x_j^{(1)})$ refers to the piece of the Hamiltonian which involves charges $x_i^{(2)}$ and $x_j^{(1)}$ and the rest of the Hamiltonian is denoted by H'.

The $x_j^{(1)}$ integration amounts to making the substitution $\vec{x}_j^{(1)} = \vec{x}_i^{(2)} + \vec{\tau}$; $d^2 x_j^{(1)} = \tau d\tau d\theta$; and integrating over angles. If we denote the latter two of integrals of equation B3 by I, then:

$$
\begin{aligned}
I &= \frac{d\tau}{\tau} \int_A \frac{d^2 x_i^{(2)}}{\tau^2} \int_0^{2\pi} d\theta \, e^{-H(\vec{x}_i^{(2)}, \vec{x}_i^{(2)} + \vec{\tau})} \\
&\times \delta\left(\frac{x_i^{(1)} - x_i^{(2)}}{\tau}\right) \delta\left(\frac{\vec{x}_i^{(2)} - \vec{x}_j^{(2)} + \vec{\tau}}{\tau}\right)
\end{aligned} \quad \text{(B4)}
$$

We assume that our gas of defects is sufficiently dilute that the following distances are much greater than the pair separation τ: (1) the distance of a particle in plane $k+m$ from our pair, (2) the distance of a particle in plane k from the positive charge $x_i^{(1)}$, and (3) the distance of a particle in plane $k + l$ from the negative charge $x_j^{(2)}$. In this dilute limit, we may make the approximation:

$$
\delta\left(\frac{\vec{x}_i^{(1)} - \vec{x}_i^{(2)}}{\tau}\right) \delta\left(\frac{\vec{x}_i^{(2)} - \vec{x}_j^{(2)} + \vec{\tau}}{\tau}\right) \approx \frac{\tau^2}{A} \delta\left(\frac{\vec{x}_i^{(1)} - \vec{x}_j^{(2)}}{\tau}\right)
$$
$$\text{(B5)}$$

We also have that $H(x_i^{(2)}, x_j^{(1)})$ is small in this limit, which allows us to expand the exponential and to leading order, the integral may be done exactly[17]. The result is:

$$
\begin{aligned}
I &= \frac{d\tau}{\tau} \delta\left(\frac{x_i^{(1)} - x_j^{(2)}}{\tau}\right)\left(2\pi - \frac{(\pi\kappa\tau^2)^2}{A}\sum_{a\neq b} e_a e_b \ln\frac{r_{ab}}{\tau}\right) \\
&\approx 2\pi \frac{d\tau}{\tau} \delta\left(\frac{x_i^{(1)} - x_j^{(2)}}{\tau}\right)
\end{aligned}
$$
$$\text{(B6)}$$

In the penultimate line, the sum refers to a sum over all charges, positive and negative, residing in the plane $k + m$. This sum term may be neglected in the large A limit, which is why, in contrast to the Kosterlitz calculation[20], the coupling strength does not vary during our RG flow (see equation 3.14). The delta function implies that the m-dipole and $(l - m)$-dipole have been combined into a larger l-dipole. Returning to our correction term:

$$
I_{klmij} \approx 2\pi \frac{d\tau}{\tau}\left[\int_{\Omega_{\tau+d\tau}^{k,l,m}} d\Omega_\tau^{k,l,m} \exp(-H)\right]
$$
$$\text{(B7)}$$

where the space $\Omega_{\tau+d\tau}^{k,l,m}$ is analogous to $\Omega_{\tau+d\tau}$, except that there is one less m-dipole in layer k; one less $(l - m)$-dipole in layer $k + m$; and one more l-dipole in layer k. What we are actually interested in is the grand partition function (equation 3.12). Because our RG procedure is consistent with the charge neutrality constraint, the various $\{I_{klmij}\}$ may be combined with different terms in the grand partition function. When we substitute into equation 3.12 and arrange terms, we find that:

$$
\begin{aligned}
\mathcal{Z} &= \sum_{\{N_{\kappa,\lambda}\}} \frac{1}{\prod_{\kappa,\lambda}(N_{\kappa,\lambda})!}\left[\int_{\Omega_{\tau+d\tau}} d\Omega_\tau \exp(-H)\right] \\
&\times \left[\prod_{\kappa,\lambda}\left(\frac{y_\lambda}{2\pi}\right)^{N_{,\lambda}} \right. \\
&+ \left. \sum_{k,l,m}\left[\prod_{\kappa,\lambda}'\left(\frac{y_\lambda}{2\pi}\right)^{N_{,\lambda}}\right] 2\pi \frac{d\tau}{\tau}\frac{y_m y_{l-m}}{(2\pi)^2} N_{k,l}\left(\frac{y_l}{2\pi}\right)^{N_{k,l}-1}\right]
\end{aligned}
$$
$$\text{(B8)}$$

The prime on the second product means that $y_l^{N_{k,l}-1}$ has been taken outside the product. If the fugacities are small, then we may write this in a more convenient way:

$$
\begin{aligned}
\mathcal{Z} &= \sum_{\{N_{k,l}\}}\left[\prod_{k,l}\frac{(y_l + \frac{d\tau}{\tau}\sum_{m=1}^{l-1} y_m y_{l-m})^{N_{,l}}}{(2\pi)^{N_{k,l}}(N_{k,l})!}\right] \\
&\times \int_{\Omega_{\tau+d\tau}} d\Omega_\tau \exp(-H)
\end{aligned}
$$
$$\text{(B9)}$$

Finally, we rescale lengths, $x \to x(1 + d\tau/\tau)^{-1}$, and find (dropping primes):

$$
\mathcal{Z} = \sum_{\{N_{k,l}\}}\left[\prod_{k,l}\frac{\left(\frac{y_l'}{2\pi}\right)^{N_{,l}}}{(N_{k,l})!}\right]\int_{\Omega_\tau} d\Omega_\tau \exp(-H) \quad \text{(B10)}
$$

where

$$
y_l' = (y_l + \frac{d\tau}{\tau}\sum_{m=1}^{l-1} y_m y_{l-m})(1 + 2\frac{d\tau}{\tau})(1 - \kappa\frac{d\tau}{\tau}) \text{ (B11)}
$$

The flow equations (3.14) follow from this.

---

[1] M. J. Harris, S. T. Bramwell, D. F. McMorrow, T. Zeiske, and K. W. Godfrey, Phys. Rev. Lett. **79**, 2554 (1997).

[2] A. P. Ramirez, A. Hayashi, R. J. Cava, R. Siddharthan,

and B. S. Shastry, Nature **399**, 333 (1999).

3 K. Matsuhira, Z. Hiroi, T. Tayama, S. Takagi, and T. Sakakibara, J. Phys. Cond. Mat. **14**, L559 (2002).

4 Z. Hiroi, K. Matsuhira, S. Takagi, T. Tayama, and T. Sakakibara, J. Phys. Soc. Jpn. **72**, 411 (2003).

5 R. Higashinaka, H. Fukazawa, and Y. Maeno, Phys. Rev. B **68**, 014415 (2003).

6 H. Fukazawa, R. G. Melko, R. Higashinaka, Y. Maeno, and M. J. P. Gingras, Phys. Rev. B **65**, 054410 (2002).

7 S. T. Bramwell, M. J. P. Gingras, Science **294**, 1495 (2001).

8 M. J. Harris, S. T. Bramwell, P. C. W. Holdsworth, and J. D. M. Champion, Phys. Rev. Lett. **81**, 4496 (1998).

9 R. Siddharthan, B. S. Shastry, A. P. Ramirez, A. Hayashi, R. J. Cava, and S. Rosenkranz, Phys. Rev. Lett. **83**, 1854 (1999); R. Siddharthan, B. S. Shastry, and A. P. Ramirez, Phys. Rev. B **63**, 184412 (2001).

10 M. Udagawa, M. Ogata, and Z. Hiroi [J. Phys. Soc. Jpn. **71**, 2365 (2002)].

11 R. Moessner and S. L. Sondhi, Phys. Rev. B **68**, 064411 (2003).

12 R. Moessner and S. L. Sondhi, Phys. Rev. B **63**, 224401 (2001).

13 S.V. Isakov, R. Moessner, and S. L. Sondhi, *in preparation.*

14 J. F. Nagle, Phys. Rev. **152**, 190 (1966).

15 J. F. Nagle, J. Math. Phys. **7**, 1484 (1966).

16 We neglect the term proportional to $\cos(2\pi h)$.

17 S. W. Pierson, Phil. Mag. B **76**, 715 (1997).

18 K. S. Raman, PhD thesis, *in preparation.*

19 P. Chaikin and T. Lubensky, *Principles of condensed matter physics*, Cambridge University Press (1995).

20 J. M. Kosterlitz, J. Phys. C **7**, 1046 (1974).

21 S. V. Isakov, PhD thesis, Stockholm 2004.

22 T. Sakakibara, T. Tayama, Z. Hiroi, K, Matsuhira, and S. Takagi, Phys. Rev. Lett. **90**, 207205 (2003).

23 J. Snyder, J. S. Slusky, R. J. Cava, and P. Schiffer, Nature **413**, 48 (2001); K. Matsuhira, Y. Hinatsu, and T. Sakakibara, J. Phys. Cond. Mat. **13**, L737 (2001).

24 B. D. Metcalf and C. P. Yang, Phys. Rev. B **18**, 2304 (1978).

25 R. J. Baxter, J. Phys. A **13**, L61 (1980); J. Stat. Phys. **26**, 427 (1981).

26 V. Ravi Chandra, S. Ramasesha, and D. Sen, cond-mat/0403555 (unpuplished).

27 J. Richter, J. Schulenburg, A. Honecker, J. Schnack, and H.-J. Schmidt, J. Phys. Cond. Mat. **16**, S779 (2004).

28 O. Derzhko and J. Richter, *work in progress.*

29 The potential of frustrated magnets for adiabatic demagnetization has been mentioned already in M. E. Zhitomirsky, Phys. Rev. B **67**, 104421 (2003).

30 J. T. Chalker and P. Chandra, private communication.

31 R. Moessner, Phys. Rev. B **57**, R5587 (1998).